

Pyridine-Based NNS Tridentate Chitosan Thiosemicarbazones and Their Copper(II) Complexes: Synthesis, Characterization, and Anticancer Activity

Hari Sharan Adhikari, Aditya Garai, Krishna Das Manandhar, and Paras Nath Yadav*

Cite This: *ACS Omega* 2022, 7, 30978–30988

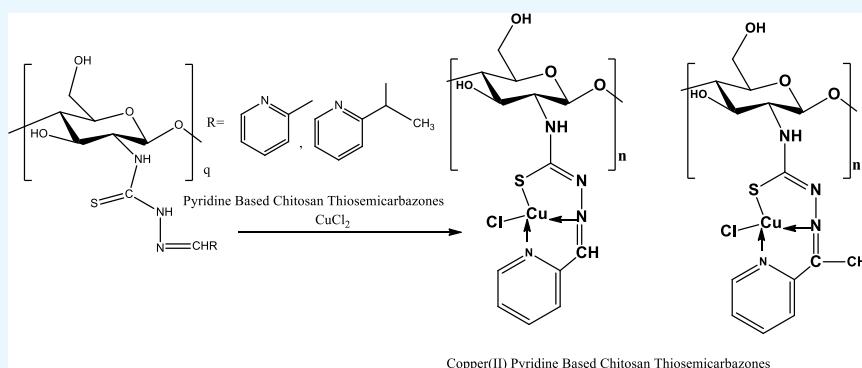
Read Online

ACCESS |

Metrics & More

Article Recommendations

Supporting Information



ABSTRACT: Chitosan-functionalized pyridine-based thiosemicarbazones and their copper(II) complexes have been found to own a substantial antiproliferative activity against the tumorigenic Madin Darby canine kidney (MDCK) and MCF-7 cancer cell lines. In the current study, chitosan oligosaccharide (CS) (87% DDA, $M_w < 3000$ Da) and crab shell chitosan (CCS) (67% DDA, M_w 350 kDa) were functionalized as chitosan pyridine-2-thiosemicarbazones and chitosan 2-acetyl pyridine-2-thiosemicarbazones, and their copper(II) complexes were synthesized. The formation of chitosan thiosemicarbazones and their NNS tridentate behavior to give the square planar copper(II) chitosan thiosemicarbazone complexes were established by spectroscopic studies, powder X-ray diffraction, elemental analysis, and magnetic moment measurements. The thermal study showed a marked stability of these derivatives before the outset of chitosan backbone degradation at 200 °C. The colorimetric MTT assay revealed a higher activity of CS thiosemicarbazones, viz., CSTSC series (IC_{50} 375–381 $\mu\text{g mL}^{-1}$ in the MDCK cell line and 281–355 $\mu\text{g mL}^{-1}$ in the MCF-7 cell line) than that of high-molecular-weight CCS thiosemicarbazones, viz., CCSTSC series (IC_{50} 335–400 $\mu\text{g mL}^{-1}$ in the MDCK cell line and 365–400 $\mu\text{g mL}^{-1}$ in the MCF-7 cell line), showing an enhanced activity with a decrease in M_w and an increase in DDA of constituent chitosan, a higher activity of both of these series of thiosemicarbazones than that of their native chitosan, viz., CS (IC_{50} 370 $\mu\text{g mL}^{-1}$ in the MCF-7 cell line and >400 $\mu\text{g mL}^{-1}$ in the MDCK cell line) and CCS ($IC_{50} > 400$ $\mu\text{g mL}^{-1}$ in both cell lines), and a higher activity of the Cu-CSTSC complexes (IC_{50} 322–342 $\mu\text{g mL}^{-1}$ in the MDCK cell line and 278–352 $\mu\text{g mL}^{-1}$ in the MCF-7 cell line) and Cu-CCSTSC complexes (IC_{50} 274–400 $\mu\text{g mL}^{-1}$ in the MDCK cell line and 231–352 $\mu\text{g mL}^{-1}$ in the MCF-7 cell line) than that of their respective ligands.

INTRODUCTION

Chitosan is a biomaterial of multipurpose applications that is obtained by partial N-deacetylation of chitin abundantly found in crab shells.¹ It shows nominal toxicity to healthy cells¹ and undergoes chemical modification through functionalization and complex formation owing to the presence of reactive amino, acetamido, and hydroxyl functionalities² to give several derivatives with enhanced anticancer activity.² Anticancer activity of the cationic polysaccharide chitosan biomaterial is generally associated with its selective permeation through the negatively charged tumor cell surfaces in a sustained release manner, causing the increase in its bioavailability in tumor cells^{2–5} followed by its inhibitory effect in cancer cells by

apoptotic,^{6–11} antiangiogenic,^{8,12} and immunoenhancing pathways^{13–17} or antioxidant defense operation.¹⁸ The enhancement in the antioxidant behavior of chitosan to scavenge and minimize the formation of free radicals upon the grafting of thiosemicarbazone¹⁹ has been attributed to weakening of intramolecular and intermolecular hydrogen bonds and

Received: May 12, 2022

Accepted: August 5, 2022

Published: August 24, 2022



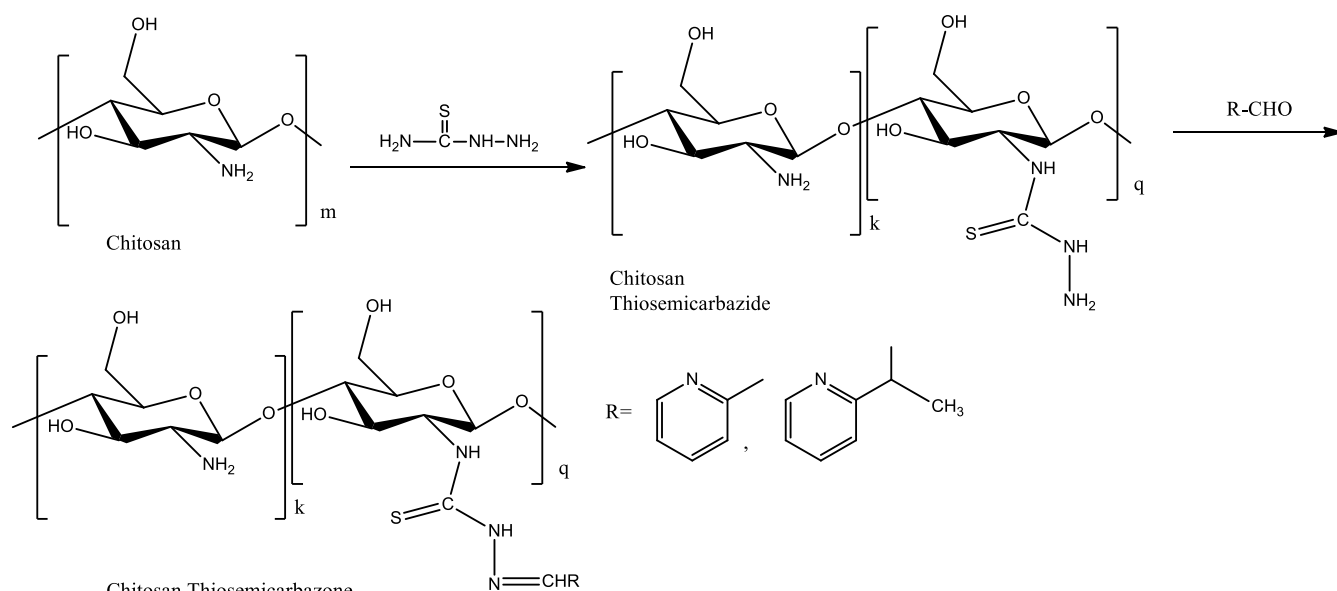


Figure 1. Synthetic route of chitosan TSCs via the formation of the chitosan thiosemicarbazide intermediate.

substantial interaction of N–H and C=S groups with the free radicals.¹⁹ This process could resist the etiological progression of age-related conditions like immune system deterioration, brain dysfunction, and cancer.^{20,21}

Thiosemicarbazones (TSCs) have been the potential anticancer drug candidates owing to their attributes like interference in the synthesis of deoxyribonucleic acid (DNA) via inhibition of ribonucleotide diphosphate reductase,^{22,23} cell cycle inhibition,²⁴ and overexpression of reactive oxygen species (ROS).²⁵ TSCs show chelation with blood transfusional ferrous ion overload that would be a factor to trigger the malignant diseases.²⁶ TSCs lend themselves to chelation with copper(II) ions accumulated in higher concentration in tumor cells due to selective permeation through the cell membrane.²⁷ These copper(II) ions acting as angiogenic factors toward the development of cancer²⁸ could be subjected to chelation with organic molecule binders to give the complexes of anti-angiogenic and tumor growth inhibiting activity.²⁸ Anticancer activity of copper(II) TSCs has been associated with their capacity to cause cellular apoptosis by generation of excess of ROS and cleave DNA through the exposure to oxidative stress.²⁷ The NNS tridentate TSCs with the carbonyl moiety of the side chain at a position that is α to heteroaromatic ring nitrogen have been found to have remarkably higher anticancer activity.²⁹ On this basis, pyridine-2-thiosemicarbazones are structurally in favor of anticancer activity, and the research motivation was to bring about the grafting of chitosan in these TSCs to get their anticancer effects synergized and further to synthesize copper(II) chitosan thiosemicarbazone complexes in search of formulations with more potent anticancer activity.

Low-molecular-weight chitosan (LMWC) with a higher degree of deacetylation (DDA) undergoes more protonation and hence more permeation through the negatively charged cancer cell membrane.¹¹ In addition, the extracellular attack of LMWC on cancer cells takes place through the process of endocytosis.^{7,30} The current work aims to comprehend the effect of molecular weight (M_w) and DDA of chitosan on anticancer activity of chitosan TSCs and their copper(II) complexes. The human breast cancer (MCF-7) cell line that possesses relatively higher negatively charged cell surfaces^{31–33}

and the Madin Darby canine kidney (MDCK) cell line with the neoplastic development by in vitro expression of immortalized cells as tumorigenic phenotypes from commercially available normal kidney cells³⁴ were preferably taken for the assessment of anticancer activity.

2. MATERIALS AND METHODS

2.1. Materials. Glacial acetic acid (Merck 99–100%), hydrochloric acid (Merck 99%), sodium hydroxide (Merck, 99%), sodium acetate (Merck), ethanol (Sigma-Aldrich, 99.80%), chitosan oligosaccharide, ($\text{C}_{12}\text{H}_{24}\text{N}_2\text{O}_9$)_n ($M_w < 3000$ Da, 87% DDA, Sisco Research Laboratories Pvt. Ltd., Maharashtra, India), pyridine-2-carboxaldehyde, 2-acetyl pyridine (Sigma-Aldrich), copper(II) chloride (Merck), sodium chloroacetate (Thermo Fisher Scientific), carbon disulphide (S D Fine-Chem limited), hydrazine monohydrate (Thermo Fisher Scientific), acetone (Thermo Fisher Scientific), ammonium hydroxide, methanol, and other analytical grade reagents were used as available with no further purification. Crab shells as chitin wastes were fetched from a local crab market of Kathmandu, Nepal.

2.2. Measurements. The Fourier transform infrared (FT-IR) spectra were taken in the powder state, with ATR-GeXPm experimentation with a BRUKER 1 003 3610 FT-IR spectrophotometer in the $4000\text{--}400\text{ cm}^{-1}$ region. The solid-state ^{13}C NMR spectra were measured at a field strength of 9.389766 [T] (400 [MHz]), with 276 scans and a contact time of 3.5 min, on a BRUKER AC-800 Delta 2 NMR spectrometer with cross-polarization. Powder X-ray diffraction (PXRD) measurements were performed with a D8 ADVANCE BRUKER diffractometer with a Cu target ($\lambda = 0.1541\text{ nm}$) at 40 KV, a scanning scope of 2θ at $0\text{--}60^\circ$, exposed for 400 S. The elemental analyses were carried out with a Thermo Finnigan FLASH EA 112CHNS microanalyzer, CHNS/NCS column PQS SS 2M 6×5 mm in an oven at 75°C , with carrier gas He (140 mL/min). The TG/DTA thermal data were taken with a DTA/TG Al crucible, at 10°C temperature rise per minute. The effective magnetic moment (μ_{eff}) of the complexes was measured using a magnetic susceptibility balance, Sherwood Scientific, Cambridge, UK, X1 range setting with the powdered sample

compactly filled up to height (L) of 1.5 cm in a weighing tube (0.8233 g). Electron paramagnetic resonance (EPR) spectra were taken at an X band frequency of 9.8577–9.8630 GHz, scan range 2000 Gs, field set 3000 Gs, Bruker biospin corp. (EMX series) model: A 200-9.5/12B/S.

The EPR spectroscopic and thermal data were taken at Sogang University, Department of Chemistry, Korea Center for Artificial Photosynthesis (KCAP), Center for Nanomaterial, Shinsu-dong, Mapogo, South Korea. The FT-IR, ^{13}C NMR spectra, elemental analyses, PXRD, and magnetic susceptibility data were taken at the Indian Institute of Science (IISc), Bangalore, India. The MTT assay against the tumorigenic MDCK cell line and MCF-7 cancer cell line was carried out at the Central Department of Biotechnology, Tribhuvan University, Kirtipur, Kathmandu, Nepal.

2.3. Experimental Section. **2.3.1. Functionalization of Chitosan as Chitosan TSCs.** The process of functionalization of chitosan as chitosan TSC involved the synthesis of chitosan thiosemicarbazide as a key intermediate. The preparation of this intermediate involved subsidiary modifications in a one-pot synthetic method via the formation of ammonium dithiocarbamate chitosan and sodium carbethoxydithiocarbamate chitosan.³⁵ First, ammonium dithiocarbamate chitosan was obtained by stirring a mixture of 1 g of chitosan and 1.5 mL of ammonia solution in ethanol at room temperature for an hour, followed by addition of 1 mL of carbon disulphide and subsequent stirring at room temperature for 2 h. Next, sodium carbethoxydithiocarbamate chitosan was obtained by successive addition of 1.42 g of sodium chloroacetate and stirring at room temperature for an hour. Then, 1 mL of hydrazine monohydrate was slowly added. The mixture was stirred at room temperature for 2 h, washed with ethanol, and filtered, and the dry brown residue of chitosan thiosemicarbazide was recovered.³⁵ In the next step, an equimolar mixture of chitosan TSC and pyridine-based carboxaldehyde with acetic acid as a catalyst was refluxed at 65 °C for 12 h, cooled to room temperature, filtered, and washed with methanol, and the dry residue of chitosan TSC was recovered.

The overall scheme of the one-pot synthesis of chitosan TSCs performed without isolation of intermediates resulted in the partial introduction of the TSC moiety and partly a Schiff's reaction of carboxaldehyde with amino groups at the C-2 position of the chitosan ring^{19,36,37} to get the chitosan-functionalized end product as shown in Figure 1.

Grafting of the thiosemicarbazone moiety in chitosan was observed in terms of the degree of substitution (DS) determined with the equation^{36–39} $\text{DS} = M_{\text{cs}} \times \%(\text{S}) / (3200 - M_{\text{tsc}} \times \%(\text{S}))$, where M_{cs} is weight of the chitosan unit ring, viz, 166 for chitosan oligosaccharide (87% DDA) and 171 for crab shell chitosan (67% DDA), M_{tsc} is weight of the TSC unit, and $\%(\text{S})$ is sulfur percentage in chitosan TSC.

2.3.1.1. Oligo-Chitosan Pyridine-2-thiosemicarbazone (CSPRTSC). Yield: 36%; color: yellowish; mp > 300 °C, decomposed into brown residue prior to melting; calc. for $\text{C}_{13}\text{H}_{16}\text{N}_4\text{O}_4\text{S}$ (unit formula wt. 324, chitosan unit 160.16) C, 48.14; H, 4.93; N, 17.28; S, 9.87%; found (for 87% DDA of chitosan) C, 44.025; H, 5.875; N, 16.069; S, 5.149%; DS: 36.28%; IR (cm^{-1} , s: strong, m: medium, w: weak): ν (O–H) and ν (N–H) stretch merged with broad translocation 3214s, ν (C=N) 1638m, ν (N–H) bend 1539s, ν (C–H) bend 1474s, ν (C=S) 1070s, 1376s, ν (pyridine ring deformation) 621m; δ (^{13}C NMR, 400 MHz, ppm) = 23.90 (CH_3), 65.99 (C6), 75.33 (C3, C5), 83.88 (C4), 103.41 (C1), 125–140 (pyridyl ring C–

H), 153.90 (HC=N–), 174.60 (C=S & C=O superimposition).

2.3.1.2. Crab Shell Chitosan Pyridine-2-thiosemicarbazone (CCSPRTSC). Yield: 34%; color: yellowish white; mp > 300 °C, decomposed prior to melting; calcd for $\text{C}_{13}\text{H}_{16}\text{N}_4\text{O}_4\text{S}$ (unit formula wt. 324, chitosan unit 160.16) C, 48.14; H, 4.93; N, 17.28; S, 9.87%; found (for 67% DDA of chitosan) C, 44.205; H, 5.324; N, 16.321; S, 4.936%; DS: 35.31%; IR (cm^{-1} , s: strong, m: medium, w: weak): ν (O–H) and ν (N–H) stretch merged with broad translocation 3257s, ν (C=N) 1653s, ν (N–H) bend 1555s, ν (C–H) bend 1478m, ν (C=S) 1036s, 1374s, ν (pyridine ring deformation) 622m; δ (^{13}C NMR, 400 MHz, ppm) = 22.92 (CH_3), 61.31 (C6), 75.58 (C3, C5), 83.31 (C4), 104.46 (C1), 125–140 (pyridyl ring C–H), 150.12 (HC=N–), 175.16 (C=S & C=O superimposition).

2.3.1.3. Oligo-Chitosan 2-Acetyl Pyridine Thiosemicarbazone (CSAPRTSC). Yield: 44%; color: yellow; mp > 300 °C, decomposed into brown residue prior to melting; calcd for $\text{C}_{14}\text{H}_{18}\text{N}_4\text{O}_4\text{S}$ (unit formula wt. 338, chitosan unit 160.16) C, 49.70; H, 5.32; N, 16.56; S, 9.46%; found (for 87% DDA of chitosan) C, 42.736; H, 5.661; N, 11.029; S, 7.010%; DS: 59.18%; IR (cm^{-1} , s: strong, m: medium, w: weak): ν (O–H) and ν (N–H) stretch merged with broad translocation 3192s, ν (C=N) 1639m, ν (N–H) bend 1504s, ν (C–H) bend 1465s, ν (C=S) 1072s, 1369s, ν (pyridine ring deformation) 620m; δ (^{13}C NMR, 400 MHz, ppm) = 24.35 (CH_3), 62.02 (C6), 75.33 (C3, C5), 84.12 (C4), 102.74 (C1), 119–160 (pyridyl ring C–H), 169.11 (HC=N–), 178.81 (C=S & C=O superimposition).

2.3.1.4. Crab Shell Chitosan 2-Acetyl Pyridine Thiosemicarbazone (CCSAPRTSC). Yield: 42%; color: yellowish white; mp > 300 °C, decomposed prior to melting; calc. for $\text{C}_{14}\text{H}_{18}\text{N}_4\text{O}_4\text{S}$ (unit formula wt. 338, chitosan unit 160.16) C, 49.70; H, 5.32; N, 16.56; S, 9.46%; found (for 67% DDA of chitosan) C, 42.051; H, 5.65; N, 10.005; S, 5.962%; DS: 47.40%; IR (cm^{-1} , s: strong, m: medium, w: weak): ν (O–H) and ν (N–H) stretch merged with broad translocation 3259s, ν (C=N) 1621s, ν (N–H) bend 1504s, ν (C–H) bend 1425s, ν (C=S) 1020s, 1376s, ν (pyridine ring deformation) 600m; δ (^{13}C NMR, 400 MHz, ppm) = 22.72 (CH_3), 61.13 (C6), 75.45 (C3, C5), 83.26 (C4), 104.16 (C1), 116–160 (pyridyl ring C–H), 164.61 (HC=N–), 174.60 (C=S & C=O superimposition).

2.3.2. Synthesis of Copper(II) Chitosan TSCs. Synthesis of copper(II) chitosan TSCs employed an extensive stirring of an equimolar mixture of chitosan thiosemicarbazone and copper(II) chloride in 1% acetic acid solution for 3 h at 65 °C and pH 6 and recovery of the complex in the dry state after filtration and oven-drying overnight at 40 °C, and this process followed subsidiary modifications^{36,37} in the method of preparation of copper(II) chitosan complexes.⁴⁰ Chlorine percentages in the complexes were determined by the reported method of potentiometric titration.⁴¹

2.3.2.1. Copper(II) Oligo-Chitosan Pyridine-2-thiosemicarbazone (Cu-CSPRTSC). Yield: 67%; color: greenish; mp > 300 °C, decomposed prior to melting; calcd for $\text{C}_{13}\text{H}_{16}\text{N}_4\text{O}_4\text{SCuCl}$ (unit formula wt. 423, chitosan unit 160.16) C, 36.87; H, 3.78; N, 13.23; S, 7.56; Cl 8.39%; found (for 87% DDA of chitosan) C, 31.75; H, 4.985; N, 9.64; S, 3.222%; estimated Cl, 12.08%; IR (cm^{-1} , s: strong, m: medium, w: weak): ν (O–H) and ν (N–H) stretch merged with broad translocation 3187s, ν (C=N) 1626m, ν (N–H) bend 1555s, ν (C=S) 1052s, 1366s, ν (pyridine ring deformation) 628m; effective magnetic moment (μ_{eff}) (B. M.):

1.79; EPR (g value): 2.10 ($\nu = 9.8623$ GHz, $B_0 = 3355$ Gs = 335.5 mT).

2.3.2.2. Copper(II) Crab Shell Chitosan Pyridine-2-thiosemicarbazone (Cu-CCSPRTSC). Yield: 66%; color: greenish; m. p. > 300 °C, decomposed prior to melting; calc. for $C_{13}H_{16}N_4O_4SCuCl$ (unit formula wt. 423, chitosan unit 160.16) C, 36.87; H, 3.78; N, 13.23; S, 7.56, Cl 8.39%; found (for 67% DDA of chitosan) C, 32.41; H, 5.427; N, 9.69; S, 3.436%; estimated Cl, 12.08%; IR (cm^{-1} , s: strong, m: medium, w: weak): ν (O–H) and ν (N–H) stretch merged with broad translocation 3187s, ν (=N) 1638m, ν (N–H) bend 1555s, ν (C=S) 1023s, 1366s, ν (pyridine ring deformation) 628m; effective magnetic moment (μ_{eff}) (B. M): 1.80; EPR (g value): 2.09 ($\nu = 9.8577$ GHz, $B_0 = 3360$ Gs = 336 mT).

2.3.2.3. Copper(II) Oligo-Chitosan 2-Acetyl Pyridine-2-thiosemicarbazone (Cu-CSAPRTSC). Yield: 72%; color: yellowish green; mp > 300 °C, decomposed prior to melting; calc. for $C_{14}H_{18}N_4O_4S CuCl$ (unit formula wt. 437, chitosan unit 160.16) C, 38.44; H, 4.11; N, 12.81; S, 7.32, Cl 8.12%; found (for 87% DDA of chitosan) C, 31.16; H, 4.397; N, 9.65; S, 4.773%; estimated Cl, 10.02%; IR (cm^{-1} , s: strong, m: medium, w: weak): ν (O–H) and ν (N–H) stretch merged with broad translocation 3260s, ν (C=N) 1604m, ν (N–H) bend 1556m, ν (C=S) 1035s, 1363s, ν (pyridine ring deformation) 628m; effective magnetic moment (μ_{eff}) (B. M): 1.89; EPR (g value): 2.08 ($\nu = 9.8623$ GHz, $B_0 = 3383$ Gs = 338.3 mT).

2.3.2.4. Copper(II) Crab Shell Chitosan 2-Acetyl Pyridine Thiosemicarbazone (Cu-CCSAPRTSC). Yield: 68%; color: yellowish green; mp > 300 °C, decomposed prior to melting; calc. for $C_{14}H_{18}N_4O_4S CuCl$ (unit formula wt. 437, chitosan unit 160.16) C, 38.44; H, 4.11; N, 12.81; S, 7.32, Cl 8.12%; found (for 67% DDA of chitosan) C, 32.41; H, 5.427; N, 9.69; S, 3.436%; estimated Cl, 10.01%; IR (cm^{-1} , s: strong, m: medium, w: weak): ν (O–H) and ν (N–H) stretch merged with broad translocation 3334s, ν (C=N) 1611s, ν (N–H) bend 1548m, ν (C=S) 1004s, 1367s, ν (pyridine ring deformation) 606m; effective magnetic moment (μ_{eff}) (B. M): 1.87; EPR (g value): 2.08 ($\nu = 9.8621$ GHz, $B_0 = 3383$ Gs = 338.3 mT).

2.3.3. Cells Culturing and Colorimetric MTT Assays. The cell line was cultured in the complete RPMI media [a mixture of 10% fetal bovine serum, 1.2% solution of antibiotics (penicillin and streptomycin), 25 mM 4-(2-hydroxyethyl)-1-piperazineethanesulfonic acid, and an incomplete media of RPMI with glutamine] and 5% carbon dioxide for 24 h.

The cells were scraped and washed well with phosphate buffer solution (PBS) to remove cellular debris, the culture medium was replaced with a fresh medium, and the cells were counted and distributed with $\sim 10^5$ cells in each well of a 96-well plate. Test solutions in dimethyl sulfoxide (DMSO) were prepared by extensive stirring and filtration of the suspension, and the concentration was calculated from the weight dissolved obtainable by subtracting the weight of undissolved residue from the weight added in 10 mL of DMSO. After the incubation of 50–400 $\mu g mL^{-1}$ test solutions for 48 h with the cultured cells, the 3-(4,5-dimethylthiazol-2-yl)-2,5-diphenyltetrazolium bromide (MTT) solution at a concentration of 5 mg/mL in PBS was added in wells. The resulting solutions were further incubated in CO_2 at 37 °C for 4 h until intracellular purple crystals of formazan were visible under a microscope. The MTT was removed, formazan crystals were dissolved in DMSO, triturated, and incubated in CO_2 at 37 °C for 30 min until the cells were lysed, and purple crystals were dissolved. Then, the intensity of the dissolved formazan crystals (purple color) was

quantified using an ELISA plate reader at 551 nm. Cell viability percentage was obtained using the relation: % viable cells = (Sample abs – Blank abs)/(Control abs – Blank abs) \times 100, where the medium only was taken as blank and the untreated cells were taken as the positive control. The concentration at the absorbance that is half of the maximum absorbance was obtained as half inhibitory concentration (IC_{50}).⁴² The inhibition ratio (IR) was determined using the relation:⁴⁰

$$IR \% = \frac{\text{control abs} - \text{sample abs}}{\text{control abs}} \times 100\%$$

3. RESULTS AND DISCUSSION

3.1. Characterization. **3.1.1. FT-IR Spectroscopy.** The FT-IR spectra of low- and high-molecular-weight chitosan-functionalized pyridine-based TSCs (Figures S1–S4) showed a merging of broad ν (O–H) and ν (N–H) in the range of 3190–3260 cm^{-1} with a broad translocation.^{39,43} The ν (C=O) of amide I at 1645 cm^{-1} ³⁹ was found to disappear, and a new band was observed in the range of 1621–1653 cm^{-1} . This was indicative of the involvement of the C=O group in imine (–C=N–) bond formation.^{39,44} The simultaneous appearance of ν (NH_2) at 1504–1556 cm^{-1} ⁴⁵ and ν (C=S) at 1020–1072 cm^{-1} ^{37,46} and 1369–1376 cm^{-1} ^{47,48} showed the partial involvement of the NH_2 group of chitosan in the formation of TSCs. The absorption bands at 600⁴⁹ and 620–622 cm^{-1} were attributed to ν (in-plane pyridine ring deformation).⁵⁰ The partial substitution of the amino group in chitosan was shown by weakening of the ν (N–H) bending peak due to primary amine and residual amide II of chitosan at 1566 cm^{-1} ¹⁹ and its negative shifting to 1504–1556 cm^{-1} . The peaks with some shifting at 1350–1474 cm^{-1} and 1057–1072 cm^{-1} were attributed to ν (C–H) and ν (C–O–C) in the chitosan ring, respectively.⁵¹ The absence of the ν (C–SH) band at 2500–2600 cm^{-1} showed more stabilization of the thiosemicarbazone moiety in the thione form.⁵² The absence or weakening of ν (thioamide CS) bands at 743–824 cm^{-1} ⁵³ also showed the transformation of thioamide into a thiosemicarbazone moiety at the C2 position of the chitosan ring.

The FT-IR spectra of copper(II) chitosan-functionalized pyridine-based TSCs (Figures S5–S8) showed the grafting of the TSC moiety to copper(II) ions. There was lowering of ν (C=N) to 1604–1638 cm^{-1} in the complex, showing the involvement of the C=N group in complex formation.⁵⁴ There was shifting of ν (C=S) to a lower frequency of 1004–1052 cm^{-1} ^{37,46} and 1363–1367 cm^{-1} ^{47,48} in the complex, showing the coordination of sulfur with metal ions. The coordination through pyridyl ring nitrogen was shown by positive shifting of ν (in-plane pyridine ring deformation) to 606–628 cm^{-1} .⁵⁰ Hence, the bonding of metal ions with TSC through azomethine nitrogen, pyridyl nitrogen, and thione sulfur was confirmed by the overall IR data.

3.1.2. Solid-State ^{13}C Nuclear Magnetic Resonance (^{13}C NMR) Spectroscopy. The chitosan ring structure and introduction of the TSC moiety at the C2 position of the ring were elucidated from solid-state ^{13}C NMR spectra of low- and high-molecular-weight chitosan-functionalized pyridine-based TSCs (Figures S9–S12). The ^{13}C NMR spectra with reduction of the C2 signal at $\delta = 55.57$ –57.63 ppm^{39,55} indicated the partial involvement of the amino group at C2, and the amino group substitution at C2 to give –N=CH was evident from $\delta = 150.12$ –169.11 ppm.³⁹ The simultaneous appearance of signals due to C=O⁵⁵ at $\delta = 174.60$ –178.81 ppm also showed the

Table 1. PXRD Data of Chitosan TSCs and Their Copper(II) Complexes: Pyridine-2-Carboxaldehyde and 2-Acetyl Pyridine Analogues

compounds	selected functionality peaks, 2θ			
	TSC crystallinity	chitosan complex crystallinity	D (nm)	C.I. (%)
CSPCTSC	20.1°, 25.5°, 28.0°, 49.8°, 50.6°		14.98	71.46
Cu-CSPCTSC	7.36°, 11.13°, 22.21°, 22.78°, 25.54°	12.92°, 21.79°, 26.68°, 29.57°	37.70	47.77
CCSPCTSC	6.28°, 9.34°, 19.08°, 26.48°		18.24	78.21
Cu-CCSPCTSC	9.40°, 23.21°	19.22°, 39.64°		
CSAPRTSC	25.51°, 27.35°, 28.05°, 34.37°, 37.73°, 49.74°		26.21	56.06
Cu-CSAPRTSC	9.41°, 16.35°, 23.48°, 32.40°	19.55°, 39.86°	16.01	30.63
CCSAPRTSC	7.06°, 12.34°, 18.92°, 21.54°, 26.06°, 27.00°		30.75	84.85
Cu-CCSAPRTSC	28.00°, 37.75°, 49.97°	20.88°, 25.51°	46.40	39.28

partial deacetylation of the acetamido moiety in chitosan. Other characteristic peaks corresponding to the ring chitosan were CH₃ (22.72–24.35 ppm), C6 (61.13–65.99 ppm), C3, C5- (75.33–75.58 ppm), C4 (83.26–84.12 ppm), and C1- (102.74–104.46 ppm).^{39,55} The pyridyl carbon signals at δ = 125–140 ppm in CSPCTSC, 125–140 ppm in CCSPCTSC, 119–160 ppm in CSAPRTSC, and 116–160 ppm in CCSAPRTSC⁵⁶ also showed the grafting of TSC with the pyridyl ring. The broadening of peak at δ = 174.60–178.81 ppm was indicative of the superimposition of C=S and C=O signals.³⁹ These results showed the formation of chitosan TSCs with partial introduction of the TSC group in chitosan.

3.1.3. Powder X-ray Diffraction (PXRD) Studies. The X-ray diffractograms of low- and high-molecular-weight chitosan-functionalized pyridine-based TSCs (Figures S13–S16) revealed several crystallinity peaks due to the TSC moiety at 2θ = 20.10–50.60° in CSPCTSC, 2θ = 6.28–26.48° in CCSPCTSC, 2θ = 25.51–49.74° in CSAPRTSC, and 2θ = 7.06–27.00° in CCSAPRTSC.^{57,58} The appearance of new peaks showing the change in the crystallinity pattern and the shifting of peaks at 10 and 20° due to chitosan^{39,59} showed the grafting of the TSC group in chitosan,³⁹ and this process of functionalization of chitosan as chitosan TSC involving the imine group formation and cleavage of intra-molecular hydrogen bonds of chitosan caused the appearance of new crystallinity peaks.⁶⁰

As calculated from the Debye–Scherrer formula,^{45,61} the particle sizes of ligands corresponding to the highest-intensity peaks in their diffraction curves in the range of 14.98–30.75 nm and the degree of crystallinity as the crystallinity index^{62–64} in the range of 56.06–84.85% showed the general trend of the increase in the crystallinity index with the decrease in particle size.

The X-ray diffractograms of the corresponding copper(II) chitosan TSCs (Figures S17–S20) showed the shifting of crystallinity patterns from the respective ligands. New peaks at 2θ = 12.92, 21.79, 26.68, and 29.57° in Cu-CSPCTSC, 2θ = 19.22 and 39.64° in Cu-CCSPCTSC, 2θ = 19.55 and 39.86° in Cu-CSAPRTSC, and 2θ = 20.88 and 25.51° in Cu-CCSAPRTSC were attributed to chelation of metal ions with different groups of TSC ligands, resulting in the formation of a new crystalline phase.^{39,61,65–67} The original crystallinity of chitosan corresponding to the peaks at 10.4 and 19.8° was not destroyed, but the crystallinity peaks were weakened and shifted due to formation of a new crystalline phase that is attributed to destruction of hydrogen bonds as a result of chelation of metal ions with amino or hydroxy groups in chitosan.⁶⁷

From the Debye–Scherrer formula,^{45,61} the particle sizes of copper(II) chitosan TSC complexes, corresponding to the maximum-intensity peak in their X-ray diffraction curves, were

found to range from 23.91–37.70 nm in pyridine-2-carboxaldehyde-based copper(II) chitosan TSCs and 16.01–46.40 nm in 2-acetyl pyridine-based copper(II) chitosan TSCs. The degree of crystallinity as the crystallinity index^{62–64} was found to be 47.77–68.87% in pyridine-2-carboxaldehyde-based copper(II) chitosan TSCs and 30.63–39.28% in 2-acetyl pyridine-based copper(II) chitosan TSCs.

The powder X-ray diffraction data of pyridine-2-carboxaldehyde and 2-acetyl pyridine chitosan TSCs and their copper(II) complexes are presented in Table 1.

3.1.4. Elemental Analysis. For the ligands CSPCTSC and CCSPCTSC, corresponding to the monomer structure of unit formula weight 324, and for the ligands CSAPRTSC and CCSAPRTSC, corresponding to the monomer structure of unit formula weight 338, the calculated percentages showed the agreement with analytically found percentages of elements when there was partial grafting of the TSC group in chitosan. This is further supported by their DS values. Corresponding to the monomer structure of unit formula weight 423 of the pyridine-2-carboxaldehyde-based complexes, and 2-acetyl pyridine-based complexes of unit formula weight 437, the analytically found percentages showed an agreement with the coordination of non-functionalized chitosan and TSC ligands with copper(II) ions. This is further supported by a higher value of estimated chlorine percentage than the calculated chlorine percentage. The DS values^{38,39} are indicative of partial substitution of the amino group of chitosan at the C2 position, and the analytically found percentages of elements in the complexes are in agreement with the simultaneous coordination of chitosan and chitosan TSC with copper(II) ions. The partial deacetylation of chitin and partial introduction of the Schiff base group into chitosan are justifiable from decreased sulfur percentage and some differences with calculated percentages of other elements as the calculated percentages were for the respective chitosan TSCs with completely deacetylated rings of chitosan.³⁹ The DS values also showed more functionalization of commercial oligo-chitosan than that of high-molecular-weight crab shell chitosan, showing more deacetylation with an increase in DDA and a decrease in M_w .

3.1.5. Thermal Studies. Thermogravimetric/differential thermal analysis (TG/DTA) curves of chitosan TSCs (Figures S21–S24) and the thermal data presented in Table 2 showed, in particular, a weight loss of 14.04% at 173 °C in CSPCTSC, 17.97% at 190 °C in CCSPCTSC, 4.41% at 72 °C followed by an abrupt weight loss of 49.92% due to the disruption of the chitosan backbone up to about 440 °C in CSAPRTSC, and 4.39% at 75 °C followed by an abrupt weight loss of 48.86% due to the disruption of the backbone up to about 440 °C in CCSAPRTSC. The thermal decomposition was attributed to

Table 2. TG/DTA Data of Thermal Events in Chitosan TSCs: Pyridine-2-Carboxaldehyde and 2-Acetyl Pyridine Analogues

compounds	temperature (°C)	weight loss (%)	thermal event	% residue at 1000 °C
CSPCTSC	173	14.04	loss of water	10
	200–1000	75	chain disruption and backbone degradation	
CCSPCTSC	190	17.97	loss of water	9
	200–1000	72	chain disruption and backbone degradation	
CSAPRTSC	72	4.41	loss of water	13
	440	49.92	abrupt disruption of backbone	
	200–1000	74	backbone degradation	
CCSAPRTSC	75	4.39	loss of water	12
	440	48.86	abrupt disruption of backbone	
	200–1000	76	backbone degradation	

the loss of water at 100–200 °C and chain degradation followed by the disruption of the chitosan backbone at 200–1000 °C. The chain degradation at 200–1000 °C caused a weight loss of 75% in CSPCTSC, 72% in CCSPCTSC, 74% in CSAPRTSC, and 76% in CCSAPRTSC. These thermal events were in agreement with the reports on loss of water in chitosan at 80–160 °C^{39,68} and decomposition of chitosan at 50–100 °C and 400–500 °C.^{69,70} Furthermore, the commercial chitosan has been reported to undergo a weight loss in two stages with 9% of weight loss owing to loss of water at 120 °C and 43% of weight loss owing to chitosan chain degradation at 500 °C,^{71–73} and in agreement to this, there was a 9.20–14.30% weight loss attributed to the loss of water at 120 °C and 65–67% weight loss as a result of chain degradation at 500 °C in chitosan TSCs. These derivatives were found to undergo more degradation than chitosan at a moderate temperature of 400–500 °C. Meanwhile, they were also found to follow the general trend of decomposition similar to that of chitosan with a rapid rate of decomposition from 100 to 400 °C and a steady rate of chain degradation, leaving about 10% CSPCTSC, 9% CCSPCTSC, 13% CSAPRTSC, and 12% CCSAPRTSC as residue of the unsaturated structure at 1000 °C. Such a thermal behavior accorded with a higher thermal stability of thiosemicarba-

zones,⁷⁴ and their DTA peaks also showed an agreement with TG weight loss in two steps of 150–400 and 400–900 °C, and an endothermic peak was attributed to the loss of water from 25–150 °C.

The TGA curves of complexes (Figures S25–S28) and the thermal data presented in Table 3 showed, in particular, a weight loss of 0.08% in Cu-CSPCTSC, 0.36% in Cu-CCSPCTSC, 5.5% in Cu-CSAPRTSC, and 0.81% in Cu-CCSAPRTSC at 200 °C and a weight loss of about 51.44% in Cu-CSPCTSC, 58.38% in Cu-CCSPCTSC, 39.15% in Cu-CSAPRTSC, and 57.58% in Cu-CCSAPRTSC at 200–500 °C. The curves showed the weight loss in three steps corresponding to a constant loss of weight up to 150–200 °C, rapid loss of weight at 200–400 °C, and again a steady loss of weight from 400–700 °C. It showed more degradation of complexes at moderate heating in the lower range of temperature from 200–500 °C and then a steady rate of decomposition, leaving about 39% Cu-CSPCTSC, 37% Cu-CCSPCTSC, 46% Cu-CSAPRTSC, and 37% Cu-CCSAPRTSC as residue of the unsaturated structure at 700 °C. These thermal events showed the standard thermal stability^{68,74} of the complexes.

3.1.6. Magnetic Susceptibility Measurement and EPR Spectroscopy. The magnetic moment (μ_{eff}) values in the range of 1.80–1.85 BM calculated from the Curie equation^{75,76} revealed that the complexes were paramagnetic, and the values fairly above the pure spin-only moment of 1.73 BM corresponded to the large spin–orbit coupling constant of cupric ions,⁷⁵ but the values <1.90 BM indicated the square planar or octahedral geometry of the complexes.⁷⁷ The low spin–spin coupling between the unpaired electrons of copper atoms was shown by the values of magnetic moment in the neighborhood of the spin-only moment of 1.73 BM corresponding to an unpaired electron.⁷⁸

The EPR spectra of complexes (Figures S29–S32) showed the absence of hyperfine splitting that was attributed to exchange broadening caused by the insufficient separation of paramagnetic centers⁷⁹ at a low frequency of the X-band at 9.8 GHz.⁷⁹ The non-resolution of hyperfine features due to copper ($S = 1/2$ and $I = 3/2$) was contributed by intermolecular spin–spin interactions and dimeric association of molecules,^{80,81} but the spectra in which the g parallel tensors were undetectable with the absence of hyperfine splitting still possessed the feature to be characterized by axial g tensors,⁸² and the spectra in correspondence to an unpaired electron in the $d_{x^2-y^2}$ orbital of Cu(II) centers showed the square planar orientation of

Table 3. TGA Data of Thermal Events in Copper(II) Chitosan TSCs: Pyridine-2-Carboxaldehyde and 2-Acetyl Pyridine Analogues

compounds	temperature (°C)	weight loss %	thermal event	% residue at 700 °C
Cu-CSPCTSC	200	0.08	loss of water	39
	200–500	51.44	disruption of the chain	
	500–700	9.52	further degradation of the backbone	
Cu-CCSPCTSC	200	0.36	loss of water	37
	200–500	58.38	disruption of the chain	
	500–700	4.41	further degradation of the backbone	
Cu-CSAPRTSC	200	5.50	loss of water	46
	200–500	39.15	disruption of the chain	
	500–700	9.40	further degradation of the backbone	
Cu-CCSAPRTSC	200	0.81	loss of water	37
	200–500	57.58	disruption of the chain	
	500–700	4.61	further degradation of the backbone	

complexes.⁸³ The g values calculated from the equation $g = h\nu/\mu_0 B_0$,⁸⁴ where $h/\mu_0 = 71.45$, $h = 6.626 \times 10^{-34}$ Js, $\mu_0 =$ Bohr magneton value of 9.27×10^{-24} J/T = 9.27×10^{-27} J/mT, ν is frequency, and B_0 is magnetic field, showed shifting from g_e (2.0023) due to spin–orbital coupling with unpaired electrons, and this spin–orbital coupling was introduced by the covalent behavior of the complex that was dependent on the density of unpaired electrons in ligand molecules.⁷⁸ The absence of the half-field peak at 1500 Gauss that was indicative of the absence of two copper centers in the same lacuna showed the mononuclear structure of complexes.⁸⁵

The overall results of characterization showed that the thione sulfur, azomethine nitrogen, pyridyl nitrogen of pyridine-2-carboxaldehyde or 2-acetyl-pyridine moieties, and one chlorine atom were used as the donor sites in coordination with copper(II) ions in the complexes that were proposed to assume the mononuclear distorted-square planar geometry (Figure 2).

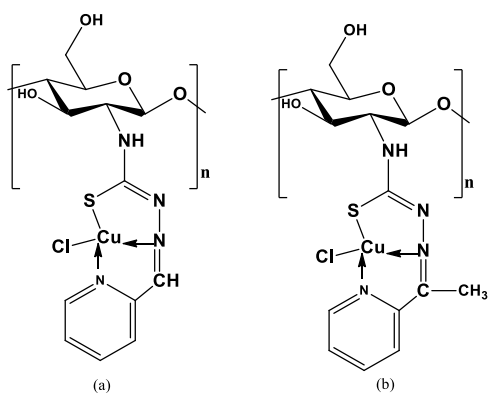


Figure 2. Proposed structure of complexes: (a). Cu-CSPCTSC and Cu-CCSPCTSC. (b). Cu-CSAPRTSC and Cu-CCSAPRTSC.

3.2. Anticancer activity. **3.2.1. MTT Assay Against the MDCK Cell Line.** The antitumor profiles against the MDCK cell line of chitosan TSCs and their copper(II) complexes are presented in Tables 4 and 5 respectively.

3.2.2. MTT Assay against the MCF-7 Cancer Cell Line. The anticancer activity profiles of chitosan TSCs and their copper(II) complexes against the MCF-7 cell line are presented in Tables 6 and 7 respectively.

3.2.3. Anticancer Activity: an Overview. The current work is a continuum of tailoring of native chitosan, viz., CS (IC_{50} 370 $\mu\text{g mL}^{-1}$ in the MCF-7 cell line and $>400 \mu\text{g mL}^{-1}$ in the MDCK cell line) and CCS ($IC_{50} > 400 \mu\text{g mL}^{-1}$ in both cell lines)³⁷ in an anticipation to get the pyridine-based novel derivatives of synergistic anticancer activity. The heteromeric unit of chitosan-functionalized TSCs was found to comprise the ingredients of non-deacetylated chitin with the unit weight 203 (13% in CSPCTSC and CSAPRTSC with 87% DDA and

33% in CCSPCTSC and CCSAPRTSC with 67% DDA), non-functionalized chitosan constituents with the unit weight 161 (55.44% in CSPCTSC with 36.28% DS, 43.35% in CCSPCTSC with 35.31% DS, 35.52% in CSAPRTSC with 59.18% DS, and 35.25% in CCSAPRTSC with 47.40% DS), and the chitosan thiosemicarbazone moiety with the unit weight 324 in CSPCTSC and CCSPCTSC and 338 in CSAPRTSC and CCSAPRTSC (31.56% in CSPCTSC, 23.65% CCSPCTSC, 51.48% in CSAPRTSC, and 31.75% in CCSAPRTSC). However, the chitosan chain depolymerization effects, protonation interferences, and variation of DDA and DS under the synthetic conditions could show an impediment toward the quantifiable determination of unit formula weight of the compounds with these structural contributions. In addition, the involvement of non-functionalized chitosan in a parallel reaction to form copper(II) chitosan also shows a hindrance to the determination of exact unit formula weight of heteropolymeric copper(II) chitosan TSCs. Therefore, the IC_{50} values have been expressed in $\mu\text{g mL}^{-1}$ instead of $\mu\text{mol mL}^{-1}$ in this study. The *in vitro* cytotoxic activity against the cell lines was statistically justifiable as the MTT assays were carried out in triplicate to observe the % inhibition by each sample solution of a particular concentration in the 50–400 $\mu\text{g mL}^{-1}$ range, and the standard deviation (S.D.) from the mean value of IC_{50} was calculated.

There was a concentration-dependent rise in IR %, and at a given concentration, oligo-chitosan TSCs were found to show more inhibition of cell growth than the high-molecular-weight crab shell chitosan. The NNS tridentate coordination of pyridine-based chitosan TSCs with copper(II) was established as a useful tool to get the derivatives with enhanced antitumor and anticancer activity. The enhancement in the activity was more in the complexes of chitosan oligosaccharide than high-molecular-weight crab shell chitosan analogues. The results are in agreement with the reports that copper(II) complexes are usually more cytotoxic than the corresponding TSC ligands probably due to their redox properties.^{86,87} Better activity of the compounds toward MCF-7 than the MDCK cell line is indicative of their selective permeability through the more negatively charged cell membranes of the cancer cells, and the electrical charge of cancer cell membrane can be altered³³ for the purpose of therapeutic intervention.

The molecular structure of pyridine-based TSCs in favor of anticancer activity,²⁹ and the reported anticancer activity of copper(II) TSC complexes via the pathways of cellular apoptosis and DNA cleavage²⁷ is indicative of the necessity of mechanistic investigation of their chitosan-functionalized analogues toward the development of chitosan drug formulations in the future. The current work of customization of biomaterial chitosan through functionalization as pyridine-based chitosan TSCs and their coordination with copper(II) and

Table 4. Inhibition Profile of MDCK Cell Line Proliferation by Commercial Chitosan TSCs (CS TSC Series) and Their Copper(II) Complexes^a

compounds	cell viability % (at 50–400 $\mu\text{g mL}^{-1}$)	$IC_{50}(\mu\text{g mL}^{-1}) \pm$ S.D.	IR % (at 50–400 $\mu\text{g mL}^{-1}$)
CSPCTSC	81–38	375 \pm 10.0	19–62
Cu-CSPCTSC	85–35	342 \pm 8.3	15–65
CSAPRTSC	81–45	381 \pm 9.8	19–55
Cu-CSAPRTSC	81–41	322 \pm 6.2	19–59

^aS.D. = Standard Deviation from the mean at $n = 3$.

Table 5. Inhibition Profile of MDCK Cell Line Proliferation by Crab Shell Chitosan TSCs (CCS TSC Series) and Their Copper(II) Complexes^a

compounds	cell viability % (at 50–400 $\mu\text{g mL}^{-1}$)	IC ₅₀ ($\mu\text{g mL}^{-1}$) \pm S.D.	IR % (at 50–400 $\mu\text{g mL}^{-1}$)
CCSPCTSC	89–57	>400	11–43
Cu-CCSPCTSC	96–57	>400	04–43
CCSAPRTSC	91–43	335 \pm 8.5	09–57
Cu-CCSAPRTSC	83–25	274 \pm 9.0	17–75

^aS.D. = Standard deviation from the mean at $n = 3$.

Table 6. Inhibition Profile of MCF-7 Cell Line Proliferation by Commercial Chitosan Thiosemicarbazones (CS TSC Series) and Their Copper(II) Complexes^a

compounds	cell viability % (at 50–400 $\mu\text{g mL}^{-1}$)	IC ₅₀ ($\mu\text{g mL}^{-1}$) \pm S.D.	IR % (at 50–400 $\mu\text{g mL}^{-1}$)
CSPCTSC	96–44	281 \pm 10.4	04–57
Cu-CSPCTSC	86–44	278 \pm 6.9	14–56
CSAPRTSC	85–48	355 \pm 10.0	15–52
Cu-CSAPRTSC	65–39	352 \pm 9.4	35–61

^aS.D. = Standard Deviation from the mean at $n = 3$.

Table 7. Inhibition Profile of MCF-7 Cell Line Proliferation by Crab Shell Chitosan Thiosemicarbazones (CCS TSC Series) and Their Copper(II) Complexes^a

compounds	cell viability % (at 50–400 $\mu\text{g mL}^{-1}$)	IC ₅₀ ($\mu\text{g mL}^{-1}$) \pm S.D.	IR % (at 50–400 $\mu\text{g mL}^{-1}$)
CCSPCTSC	78–51	>400	22–49
Cu-CCSPCTSC	70–18	231 \pm 9.0	30–82
CCSAPRTSC	69–42	365 \pm 9.6	31–58
Cu-CCSAPRTSC	69–39	352 \pm 8.0	46–62

^aS.D. = Standard Deviation from the mean at $n = 3$.

the assessment of anticancer activity of these derivatives could generate a point to start with the mechanistic investigation of their anticancer activity.

4. CONCLUSIONS

A one-pot synthetic approach of chitosan tailoring was utilized to synthesize pyridine-based chitosan TSCs, and the preparation of copper(II) chitosan TSC complexes involved coordination of NNS tridentate ligands with copper(II) ions. Both the chitosan-functionalized TSC ligands and the respective complexes were found structurally favorable toward the *in vitro* inhibition of tumorigenic MDCK and MCF-7 cancer cell line proliferation. The study revealed a higher activity of copper(II) chitosan TSCs than that of free ligands, analogous anticancer effects upon the grafting of pyridine-2-carboxaldehyde and 2-acetyl pyridine on chitosan, and more inhibitory effects in MCF-7 cancer cells than in tumorigenic MDCK cells. The study also showed an irregular cytotoxic activity enhancement upon the complex formation with high-molecular-weight chitosan derivatives but a regular enhancement upon the complex formation with LMWC analogues. In particular, the activity was found enhanced, irrespective of the molecular weight and DDA of chitosan.

■ ASSOCIATED CONTENT

SI Supporting Information


The Supporting Information is available free of charge at <https://pubs.acs.org/doi/10.1021/acsomega.2c02966>.

Characterizing spectra, X-ray diffractograms and thermoanalytical curves of chitosan oligosaccharides and high-molecular-weight crab shell chitosan-functionalized pyridine-based TSCs and their copper(II) complexes, *viz.*, FT-IR spectra of chitosan pyridine-2-thiosemicarbazones, chitosan 2-acetyl pyridine-2-thiosemicarbazones, and the

corresponding copper(II) chitosan TSC complexes, ¹³C NMR spectra of chitosan pyridine-2-thiosemicarbazones and chitosan 2-acetyl pyridine-2-thiosemicarbazones, powder X-ray diffractograms of chitosan pyridine-2-thiosemicarbazones, chitosan 2-acetyl pyridine-2-thiosemicarbazones, and the corresponding copper(II) chitosan thiosemicarbazone complexes, TG/DTA curves of chitosan pyridine-2-thiosemicarbazones and chitosan 2-acetyl pyridine-2-thiosemicarbazones, TG curves of copper(II) chitosan pyridine-2-thiosemicarbazones and copper(II) chitosan 2-acetyl pyridine-2-thiosemicarbazones, and EPR spectra of copper(II) chitosan pyridine-2-thiosemicarbazones and copper(II) chitosan 2-acetyl pyridine-2-thiosemicarbazones (PDF)

■ AUTHOR INFORMATION

Corresponding Author

Paras Nath Yadav – Central Department of Chemistry, Tribhuvan University, Kathmandu 44600, Nepal;
 orcid.org/0000-0002-0661-4287; Email: pnayadav219@gmail.com

Authors

Hari Sharan Adhikari – Institute of Engineering, Department of Applied Sciences, Tribhuvan University, Pokhara 33700, Nepal

Aditya Garai – Department of Inorganic and Physical Chemistry, Indian Institute of Science, Bangalore 560012, India

Krishna Das Manandhar – Central Department of Biotechnology, Tribhuvan University, Kathmandu 44600, Nepal

Complete contact information is available at:

<https://pubs.acs.org/10.1021/acsomega.2c02966>

Notes

The authors declare no competing financial interest.

ACKNOWLEDGMENTS

We acknowledge the Nepal Academy of Science and Technology (NAST) and the Indian National Science Academy (INSA) for research fellowship to the first author. We thank Professor A. R. Chakravarty, Department of Inorganic and Physical Chemistry, Indian Institute of Science, Bangalore, India, for overall guidance in characterization work, Dr Agni Koirala, Sogang University, Department of Chemistry, KCAP, Center for Nanomaterial, Shinsu-dong, Mapogo, South Korea, for EPR spectroscopic and thermal data, and the Central Department of Biotechnology, Tribhuvan University, Kathmandu, Nepal for anticancer screening.

REFERENCES

- (1) Wimardhani, Y. S.; Suniarti, D. F.; Freisleben, H. J.; Wanandi, S. I.; Ikeda, M. A. Cytotoxic effects of chitosan against oral cancer cell lines is molecular-weight-dependent and cell type-specific. *Int. J. Oral Res.* **2012**, *3*, 1–10.
- (2) Adhikari, H. S.; Yadav, P. N. Anticancer Activity of Chitosan, Chitosan Derivatives, and Their Mechanism of Action. *Int. J. Biomater.* **2018**, *2018*, 2952085.
- (3) Gavhane, Y. N.; Gurav, A. S.; Yadav, A. V. Chitosan and Its Applications: A Review of Literature. *Int. J. Res. Pharm. Biomed. Sci.* **2013**, *4*, 312–331.
- (4) Zhang, H.; Wu, F.; Li, Y.; Yang, X.; Huang, J.; Lv, T.; Zhang, Y.; Chen, J.; Chen, H.; Gao, Y.; Liu, G.; Jia, L. Chitosan-based nanoparticles for improved anticancer efficacy and bioavailability of mifepristone. *Beilstein J. Nanotechnol.* **2016**, *7*, 1861–1870.
- (5) Thanou, M.; Verhoef, J. C.; Junginger, H. E. Chitosan and its derivatives as intestinal absorption enhancers. *Adv. Drug Delivery Rev.* **2001**, *50*, S91–S101.
- (6) Park, J. K.; Chung, M. J.; Choi, H. N.; Park, Y. I. Effects of the molecular weight and the degree of deacetylation of chitosan oligosaccharides on antitumor activity. *Int. J. Mol. Sci.* **2011**, *12*, 266–277.
- (7) Wimardhani, Y. S.; Suniarti, D. F.; Freisleben, H. J.; Wanandi, S. I.; Siregar, N. C.; Ikeda, M. A. Chitosan exerts anticancer activity through induction of apoptosis and cell cycle arrest in oral cancer cells. *J. Oral Sci.* **2014**, *56*, 119–126.
- (8) Xu, Y.; Wen, Z.; Xu, Z. Chitosan nanoparticles inhibit the growth of human hepatocellular carcinoma xenografts through an antiangiogenic mechanism. *Anticancer Res.* **2009**, *29*, 5103–5109.
- (9) Sugano, M.; Fujikawa, T.; Hiratsuji, Y.; Nakashima, K.; Fukuda, N.; Hasegawa, Y. A novel use of chitosan as a hypocholesterolemic agent in rats. *Am. J. Clin. Nutr.* **1980**, *33*, 787–793.
- (10) Takimoto, H.; Hasegawa, M.; Yagi, K.; Nakamura, T.; Sakaeda, T.; Hirai, M. Proapoptotic effect of a dietary supplement: water soluble chitosan activates caspase-8 and modulating death receptor expression. *Drug Metab. Pharmacokinet.* **2004**, *19*, 76–82.
- (11) Zhang, J.; Xia, W.; Liu, P.; Cheng, Q.; Tah, T.; Gu, W.; Li, B. Chitosan modification and pharmaceutical/biomedical applications. *Mar. Drugs* **2010**, *8*, 1962–1987.
- (12) Jiang, Z.; Han, B.; Li, H.; Yang, Y.; Liu, W. Carboxymethyl chitosan represses tumor angiogenesis in vitro and in vivo. *Carbohydr. Polym.* **2015**, *129*, 1–8.
- (13) Maeda, Y.; Kimura, Y. Antitumor Effects of Various Low-Molecular-Weight Chitosans Are Due to Increased Natural Killer Activity of Intestinal Intraepithelial Lymphocytes in Sarcoma 180-Bearing Mice. *J. Nutr.* **2004**, *134*, 945–950.
- (14) Kuppusamy, S.; Karuppaiah, J. Screening of Antiproliferative Effect of Chitosan on Tumor Growth and Metastasis in T24 Urinary Bladder Cancer Cell Line. *Austral-Asian J. Cancer* **2013**, *12*, 145–149.
- (15) Hosseinzadeh, H.; Atyabi, F.; Dinarvand, R.; Ostad, S. N. Chitosan-Pluronic nanoparticles as oral delivery of anticancer gemcitabine: preparation and in vitro study. *Int. J. Nanomed.* **2012**, *7*, 1851–1863.
- (16) Shen, K.-T.; Chen, M.-H.; Chan, H.-Y.; Jeng, J.-H.; Wang, Y.-J. Inhibitory effects of chitoooligosaccharides on tumor growth and metastasis. *Food Chem. Toxicol.* **2009**, *47*, 1864–1871.
- (17) Qin, C.; Zhou, B.; Zeng, L.; Zhang, Z.; Liu, Y.; Du, Y.; Xiao, L. The physicochemical properties and antitumor activity of cellulase-treated chitosan. *Food Chem.* **2004**, *84*, 107–115.
- (18) Fernandes, J. C.; Sereno, J.; Garrido, P.; Parada, B.; Cunha, M. F. X.; Reis, F.; Pintado, M. E.; Santos-Silva, A. Inhibition of bladder tumor growth by chitoooligosaccharides in an experimental carcinogenesis model. *Mar. Drugs* **2012**, *10*, 2661–2675.
- (19) Zhong, Z.; Zhong, Z.; Xing, R.; Li, P.; Mo, G. The preparation and antioxidant activity of 2-[phenylhydrazine (or hydrazine)-thiosemicarbazone]-chitosan. *Int. J. Biol. Macromol.* **2010**, *47*, 93–97.
- (20) McCord, J. M. The evolution of free radicals and oxidative stress. *Am. J. Med.* **2000**, *108*, 652–659.
- (21) Rao, A. L.; Bharani, M.; Pallavi, V. Role of antioxidants and free radicals in health and disease. *Adv. Pharmacol. Toxicol.* **2006**, *7*, 29–38.
- (22) Finch, R. A.; Liu, M.-C.; Grill, S. P.; Rose, W. C.; Loomis, R.; Vasquez, K. M.; Cheng, Y.; Sartorelli, A. C. Triapine (3-aminopyridine-2-carboxaldehyde-thiosemicarbazone): a potent inhibitor of ribonucleotide reductase activity with broad spectrum antitumor activity. *Biochem. Pharmacol.* **2000**, *59*, 983–991.
- (23) Gojo, I.; Tidwell, M. L.; Greer, J.; Takebe, N.; Seiter, K.; Pochron, M. F.; Johnson, B.; Sznol, M.; Karp, J. E. Phase I and pharmacokinetic study of triapine, a potent ribonucleotide reductase inhibitor, in adults with advanced hematologic malignancies. *Leuk. Res.* **2007**, *31*, 1165–1173.
- (24) Rao, V. A.; Klein, S. R.; Agama, K. K.; Toyoda, E.; Adachi, N.; Pommier, Y.; Shacter, E. B. The Iron Chelator Dp44mT Causes DNA Damage and Selective Inhibition of Topoisomerase II α in Breast Cancer Cells. *Cancer Res.* **2009**, *69*, 948–957.
- (25) Malarz, K.; Mrozek-Wilczkiewicz, A.; Serda, M.; Rejmund, M.; Polanski, J.; Musiol, R. The role of oxidative stress in activity of anticancer thiosemicarbazones. *Oncotarget* **2018**, *9*, 17689–17710.
- (26) Kontoghiorghes, C. N.; Kolnagou, A.; Kontoghiorghes, G. J. Phytochelators intended for clinical use in iron overload, other diseases of iron imbalance and free radical pathology. *Molecules* **2015**, *20*, 20841–20872.
- (27) Singh, N. K.; Kumbhar, A. A.; Pokharel, Y. R.; Yadav, P. N. Anticancer potency of copper(II) complexes of thiosemicarbazones. *J. Inorg. Biochem.* **2020**, *210*, 111134.
- (28) Wang, F.; Jiao, P.; Qi, M.; Frezza, M.; Dou, Q. P.; Yan, B. Turning Tumor-Promoting Copper into an Anti-Cancer Weapon via High-Throughput Chemistry. *Curr. Med. Chem.* **2010**, *17*, 2685–2698.
- (29) Shakya, B.; Yadav, P. N. Thiosemicarbazones as Potent Anticancer Agents and their Modes of Action. *Mini-Rev. Med. Chem.* **2020**, *20*, 638–661.
- (30) Huang, M.; Khor, E.; Lim, L.-Y. Uptake and cytotoxicity of chitosan molecules and nanoparticles: effects of molecular weight and degree of deacetylation. *Pharm. Res.* **2004**, *21*, 344–353.
- (31) Comsa, S.; Cimpean, A. M.; Raica, M. The Story of MCF-7 Breast Cancer Cell Line: 40 years of Experience in Research. *Anticancer Res.* **2015**, *35*, 3147–3154.
- (32) Faris, T.; Harisa, G. I.; Alanazi, F. K.; Badran, M. M.; Alotaibi, A. M.; Almane, H.; Alqahtani, A. S.; Samy, A. M. Cytotoxicity of Chitosan Ultrafine Nanoshuttles on the MCF-7 Cell Line as a Surrogate Model for Breast Cancer. *Curr. Drug Delivery* **2021**, *18*, 19–30.
- (33) Zhou, Y.; Wong, C.-O.; Cho, K.-j.; van der Hoeven, D.; Liang, H.; Thakur, D. P.; Luo, J.; Babic, M.; Zinsmaier, K. E.; Zhu, M. X.; Hu, H.; Venkatachalam, K.; Hancock, J. F. Membrane potential modulates plasma membrane phospholipid dynamics and K-Ras signaling. *Science* **2015**, *349*, 873–876.
- (34) Omeir, R. L.; Teferedegne, B.; Foseh, G. S.; Beren, J. J.; Snoy, P. J.; Brinster, L. R.; Cook, J. L.; Peden, K.; Lewis, A. M., Jr Heterogeneity

of the tumorigenic phenotype expressed by Madin-Darby canine kidney cells. *Comp. Med.* **2011**, *61*, 243–250.

(35) Muzzarelli, R. A. A.; Tanfani, F.; Mariotti, S.; Emanuelli, M. Preparation and characteristic properties of dithiocarbamate chitosan, a chelating polymer. *Carbohydr. Res.* **1982**, *104*, 235–243.

(36) Adhikari, H. S.; Garai, A.; Khanal, C.; Adhikari, R.; Yadav, P. N. Imidazole-2-carboxaldehyde Chitosan Thiosemicarbazones and their Copper(II) Complexes: Synthesis, Characterization and Antitumor Activity against Madin-Darby Canine Kidney Cell Line. *Asian J. Chem.* **2021**, *33*, 969–976.

(37) Adhikari, H. S.; Garai, A.; Thapa, M.; Adhikari, R.; Yadav, P. N. Chitosan functionalized thiophene-2-thiosemicarbazones, and their copper(II) complexes: synthesis, characterization, and anticancer activity. *J. Macromol. Sci., Part A: Pure Appl. Chem.* **2022**, *59*, 211–227.

(38) Pires, N. R.; Cunha, P. L. R.; Maciel, J. S.; Angelim, A. L.; Melo, V. M. M.; de Paula, R. C. M.; Feitosa, J. P. A. Sulfated chitosan as tear substitute with no antimicrobial activity. *Carbohydr. Polym.* **2013**, *91*, 92–99.

(39) Qin, Y.; Xing, R.; Liu, S.; Li, K.; Meng, X.; Li, R.; Cui, J.; Li, B.; Li, P. Novel thiosemicarbazone chitosan derivatives: Preparation, characterization, and antifungal activity. *Carbohydr. Polym.* **2012**, *87*, 2664–2670.

(40) Zheng, Y.; Yi, Y.; Qi, Y.; Wang, Y.; Zhang, W.; Du, M. Preparation of chitosan-copper complexes and their antitumor activity. *Bioorg. Med. Chem. Lett.* **2006**, *16*, 4127–4129.

(41) Tiwari, D.; Basnet, K.; Lamichhane, J.; Niraula, P.; Bhandari, S.; Yadav, P. N. Copper Complexes of Imidazole-2-carbaldehyde N(4)-Substituted Thiosemicarbazones: Synthesis, Characterization and Antimicrobial Activity. *Asian J. Chem.* **2016**, *28*, 2793–2797.

(42) Kumar, P.; Nagarajan, A.; Uchil, P. D. Analysis of Cell Viability by the MTT Assay. *Cold Spring Harb. Protoc.* **2018**, *2018*, pdb.prot095505–471.

(43) Zhong, Z.; Aotegen, B.; Xu, H. The influence of the different inductivity of acetyl phenyl thiosemicarbazone-chitosan on antimicrobial activities. *Int. J. Biol. Macromol.* **2011**, *48*, 713–719.

(44) Yadav, P. N.; Demertzis, M. A.; Kovala-Demertzi, D.; Castineiras, A.; West, D. X. Synthesis, solution and spectral studies of palladium(II) complexes with 2-hydroxyacetophenone N(3)-propylthiosemicarbazone. Crystal structure of a tripalladium complex. *Inorg. Chim. Acta.* **2002**, *332*, 204–209.

(45) Kucukgulmez, A.; Celik, M.; Yanar, Y.; Sen, D.; Polat, H.; Kadak, A. E. Physicochemical characterization of chitosan extracted from *Metapenaeus stebbingi* shells. *Food Chem.* **2011**, *126*, 1144–1148.

(46) Yamaguchi, A.; Penland, R. B.; Mizushima, S.; Lane, T. J.; Curran, C.; Quagliano, J. V. Infrared Absorption Spectra of Inorganic Coordination Complexes. XIV. Infrared Studies of Some Metal Thiourea Complexes I. *J. Am. Chem. Soc.* **1958**, *80*, 527–529.

(47) Aneesrahman, K. N.; Ramaiah, K.; Rohini, G.; Steffy, G. P.; Bhuvanesh, N. S. P.; Sreeranth, A. Synthesis and characterisations of copper(II) complexes of 5-methoxyisatin thiosemicarbazones: Effect of N-terminal substitution on DNA/protein binding and biological activities. *Inorg. Chim. Acta.* **2019**, *492*, 131–141.

(48) Joseph, M.; Kuriakose, M.; Kurup, M. R. P.; Suresh, E.; Kishore, A.; Bhat, S. G. Structural, antimicrobial and spectral studies of copper(II) complexes of 2-benzoylpyridine N(4)-phenyl thiosemicarbazone. *Polyhedron* **2006**, *25*, 61–70.

(49) Nanbu, K.; Kitamura, F.; Ohsaka, T.; Tokuda, K. Adsorption of pyridine on a polycrystalline gold electrode surface studied by infrared reflection absorption spectroscopy. *J. Electroanal. Chem.* **1999**, *470*, 136–143.

(50) Rapheal, P. F.; Manoj, E.; Prathapachandra Kurup, M. R. Copper(II) complexes of N(4)-substituted thiosemicarbazones derived from pyridine-2-carbaldehyde: Crystal structure of a binuclear complex. *Polyhedron* **2007**, *26*, 818–828.

(51) Yadav, M. K.; Pokhrel, S.; Yadav, P. N. Novel chitosan derivatives of 2-imidazolecarboxaldehyde and 2-thiophenecarboxaldehyde and their antibacterial activity. *J. Macromol. Sci., Part A: Pure Appl. Chem.* **2020**, *57*, 703–710.

(52) Bharti, N.; Shailendra; Sharma, S.; Naqvi, F.; Azam, A. New palladium(II) complexes of 5-nitrothiophene-2-carboxaldehyde thiosemicarbazones. *Bioorg. Med. Chem.* **2003**, *11*, 2923–2929.

(53) Kovala-Demertzi, D.; Demertzis, M.; Yadav, P. N.; Castineiras, A.; West, D. X. Preparation, spectral and structural characterization of (2-benzoylpyridine N(4)-methyl-N(4)-phenylthiosemicarbazone) chloropalladium(II). *Transit. Met. Chem.* **1999**, *24*, 642–647.

(54) Demertzis, M. A.; Yadav, P. N.; Kovala-Demertzi, D. Palladium(II) Complexes of the Thiosemicarbazone and N-Ethylthiosemicarbazone of 3-Hydroxypyridine-2-carbaldehyde: Synthesis, Properties, and X-Ray Crystal Structure. *Helv. Chim. Acta* **2006**, *89*, 1959–1970.

(55) Wang, J.; Jiang, J.-Z.; Chen, W.; Bai, Z.-W. Data of ¹H/¹³C NMR spectra and degree of substitution for chitosan alkyl urea. *Data Brief* **2016**, *7*, 1228–1236.

(56) Li, Q.; Ren, J.; Dong, F.; Feng, Y.; Gu, G.; Guo, Z. Synthesis and antifungal activity of thiazazole-functionalized chitosan derivatives. *Carbohydr. Res.* **2013**, *373*, 103–107.

(57) Hanumantharao, R.; Kalainathan, S.; Bhagavannarayana, G. Growth, spectral, optical, thermal, crystallization perfection and nonlinear optical studies of novel nonlinear optical crystal-Urea thiosemicarbazone monohydrate. *Spectrochim. Acta, Part A* **2012**, *91*, 345–351.

(58) Santhakumari, R.; Ramamurthi, K.; Vasuki, G.; Yamin, B. M.; Bhagavannarayana, G. Synthesis and spectral characterization of acetophenone thiosemicarbazone-A nonlinear optical material. *Spectrochim. Acta, Part A* **2010**, *76*, 369–375.

(59) Ramya, R.; Sudha, P. N.; Mahalakshmi, J. Preparation and Characterization of Chitosan Binary Blend. *Int. J. Sci. Res. Publ.* **2012**, *2*, 1–9.

(60) Jiao, T. F.; Zhou, J.; Zhou, J.-X.; Gao, L.-H.; Xing, Y. Y.; Li, X.-H. Synthesis and Characterization of Chitosan-based Schiff Base Compounds with Aromatic Substituent Groups. *Iran. Polym. J.* **2011**, *20*, 123–136.

(61) Dehaghi, S. M.; Rahmanifar, B.; Moradi, A. M.; Azar, P. A. Removal of permethrin pesticide from water by chitosan-zinc oxide nanoparticles composite as an adsorbent. *J. Saudi Chem. Soc.* **2014**, *18*, 348–355.

(62) Kumirska, J.; Czerwicka, M.; Kaczyński, Z.; Bychowska, A.; Brzozowski, K.; Thöming, J.; Stepnowski, P. Application of spectroscopic Methods for Structural Analysis of Chitin and Chitosan. *Mar. Drugs* **2010**, *8*, 1567–1636.

(63) Lomadze, N.; Schneider, H. J. A. A chitosan-based chemo-mechanical polymer triggered by stacking effects with aromatic effectors including amino acid derivatives. *Tetrahedron* **2005**, *61*, 8694–8698.

(64) Zhang, Y. Q.; Xue, C. H.; Xue, Y.; Gao, R. C.; Zhang, X. L. Determination of the degree of deacetylation of chitin and chitosan by X-ray powder diffraction. *Carbohydr. Res.* **2005**, *340*, 1914–1917.

(65) Antony, R.; David, S.; Karuppasamy, K.; Saravanan, K.; Thanikaikarasan, S.; Balakumar, S. Structural, Surface, Thermal and Catalytic Properties of Chitosan Supported Cu(II) Mixed Ligand Complex Materials. *J. Surf. Eng. Mater. Adv. Technol.* **2012**, *02*, 284–291.

(66) Mekahlia, S.; Bouzid, B. Chitosan-Copper (II) complex as antibacterial agent: synthesis, characterization and coordinating bond-activity correlation study. *Phys. Procedia* **2009**, *2*, 1045–1053.

(67) Wang, X.; Du, Y.; Fan, L.; Liu, H.; Hu, Y. Chitosan-metal complexes as antimicrobial agent: Synthesis, characterization and Structure-activity study. *Polym. Bull.* **2005**, *55*, 105–113.

(68) Kittur, F. S.; Harish Prashanth, K. V. H.; Udaya Sankar, K. U.; Tharanathan, R. N. Characterization of chitin, chitosan and their carboxymethyl derivatives by differential scanning calorimetry. *Carbohydr. Polym.* **2002**, *49*, 185–193.

(69) de Andrade, S. M. B.; Ladchumananandasivam, R.; Rocha, B.; Belarmino, D.; Galvão, A. The use of exoskeletons of shrimp (*Litopenaeus vanammei*) and crab (*Ucides cordatus*) for the extraction of chitosan and production of nanomembrane. *Mater. Sci. Appl.* **2012**, *3*, 495–508.

(70) Kumari, S.; Kumar Annamareddy, S. H. K.; Abanti, S.; Kumar Rath, P. K. Physicochemical properties and characterization of chitosan synthesized from fish scales, crab and shrimp shells. *Int. J. Biol. Macromol.* **2017**, *104*, 1697–1705.

(71) Chethan, P. D.; Vishalakshi, B.; Sathish, L.; Ananda, K.; Poojary, B. Preparation of substituted quaternized arylfuran chitosan derivatives and their antimicrobial activity. *Int. J. Biol. Macromol.* **2013**, *59*, 158–164.

(72) Debritto, D.; Campana-Filho, S. P. A kinetic study on the thermal degradation of N,N,N-trimethylchitosan. *Polym. Degrad. Stab.* **2004**, *84*, 353–361.

(73) Xu, T.; Xin, M.; Li, M.; Huang, H.; Zhou, S. Synthesis, characteristic and antibacterial activity of N,N,N-trimethyl chitosan and its carboxymethyl derivatives. *Carbohydr. Polym.* **2010**, *81*, 931–936.

(74) Qu, X.; Wirsén, A.; Albertsson, A. Effect of lactic/glycolic acid side chains on the thermal degradation kinetics of chitosan derivatives. *Polymer* **2000**, *41*, 4841–4847.

(75) Djordjevic, C. Magnetic Susceptibilities of Some Square Four-Covalent and Tetragonal Six-Covalent Complexes of Divalent Copper. *Croat. Chem. Acta* **1960**, *32*, 183–187.

(76) Syamal, A.; Kale, K. S. Magnetic Properties of Copper(II) Complexes of Schiff Bases Derived from Pyrrole-2-aldehyde and Isopropanolamine/2-amino-2-methylpropanol. *Curr. Sci.* **1975**, *44*, 256–258.

(77) Figgis, B. N. Magnetic Properties of Spin-Free Transition Series Complexes. *Nature* **1958**, *182*, 1568–1570.

(78) Ahmed, A.; Lal, R. A. Synthesis, characterization and electrochemical studies of copper(II) complexes derived from succinoyl- and adipoyldihydrazones. *Arabian J. Chem.* **2017**, *10*, S901–S908.

(79) Farra, R.; Thiel, K.; Winter, A.; Klamroth, T.; Pöppel, A.; Kelling, A.; Schilde, U.; Taubert, A.; Strauch, P. Tetrahalidocuprates(ii)-structure and EPR spectroscopy. Part 1: Tetrabromidocuprates(ii). *New J. Chem.* **2011**, *35*, 2793–2803.

(80) Bhadbhade, M. M.; Srinivas, D. Effects on molecular association, chelate conformation, and reactivity toward substitution in copper Cu(S-X-salen) complexes, salen²⁻ = N,N'-ethylenebis(salicylidaminato), X = H, CH₃O, and Cl: synthesis, x-ray structures, and EPR investigations. *Inorg. Chem.* **1993**, *32*, 5458–5466.

(81) Suresh, E.; Bhadbhade, M. M.; Srinivas, D. Molecular association, chelate conformation and reactivity correlations in substituted o-phenylenebis(salicylidinato)copper(II) complexes: UV-visible, EPR and X-ray structural investigations. *Polyhedron* **1996**, *15*, 4133–4144.

(82) Bennur, T. H.; Srinivas, D.; Ratnasamy, P. EPR spectroscopy of copper and manganese complexes encapsulated in zeolites. *Microporous Mesoporous Mater.* **2001**, *48*, 111–118.

(83) Garrriba, E.; Micera, G. The Determination of the Geometry of Cu(II) Complexes: An EPR Spectroscopy Experiment. *J. Chem. Educ.* **2006**, *83*, 1229–1232.

(84) Segal, B. G.; Kaplan, M.; Fraenkel, G. K. Measurement of g Values in the Electron Spin Resonance Spectra of Free Radicals. *J. Chem. Phys.* **1965**, *43*, 4191–4200.

(85) Patel, A.; Sadasivan, R. Microwave assisted one pot synthesis and characterization of Cesium salt of di-copper substituted phosphotungstate and its application in the selective epoxidation of cis-cyclooctene with tert-butyl hydroperoxide. *Inorg. Chim. Acta.* **2017**, *458*, 101–108.

(86) Ferrari, M. B.; Capacchi, S.; Pelosi, G.; Reffo, G.; Tarasconi, P.; Albertini, R.; Pinelli, S.; Lunghi, P. Synthesis, structural characterization and biological activity of helical thiosemicarbazone monohydrate and a copper(II) complex of salicylaldehyde thiosemicarbazone. *Inorg. Chim. Acta.* **1999**, *286*, 134–141.

(87) West, D. X.; Liberta, A. E. Thiosemicarbazone complexes of copper(II): structural and biological studies. *Coord. Chem. Rev.* **1993**, *123*, 49–71.

NOTE ADDED AFTER ASAP PUBLICATION

This paper published ASAP on August 24, 2022, with an error on page four of document; 400 $\mu\text{mol L}^{-1}$ was updated to $\mu\text{g mL}^{-1}$, and the corrected version was reposted on August 25, 2022.

Recommended by ACS

Potent Inhibition of Thioredoxin Reductase by the Rh Derivatives of Anticancer M(arene/Cp*)(NHC)Cl₂ Complexes

Dianna Truong, Christian G. Hartinger, *et al.*

FEBRUARY 19, 2020
INORGANIC CHEMISTRY

READ 

Antiproliferative Activities of Diimine-Based Mixed Ligand Copper(II) Complexes

Nazanin Kordestani, Olivier Blacque, *et al.*

JANUARY 08, 2020
ACS COMBINATORIAL SCIENCE

READ 

Novel Copper-Containing Cytotoxic Agents Based on 2-Thioxoimidazolones

Olga O. Krasnovskaya, Alexander G. Majouga, *et al.*

SEPTEMBER 28, 2020
JOURNAL OF MEDICINAL CHEMISTRY

READ 

Synthesis and Characterization of the Nanogold-Bound Ternary Copper(II) Complex of Phenanthroline and Cysteine as Potential Anticancer Agents

Ahmad Junaid, Ing Hong Ooi, *et al.*

JULY 19, 2022
ACS OMEGA

READ 

Get More Suggestions >